

Multi-arc Orbit Determination to determine Rosetta trajectory and 67P physical parameters

By Bernard GODARD,¹⁾ Frank BUDNIK,²⁾ Gabriele BELLEI,³⁾ Pablo MUÑOZ,⁴⁾ and Trevor MORLEY.¹⁾

¹⁾Telespazio VEGA Deutschland GmbH, located at ESOC, Germany

²⁾ESA/ESOC, Germany

³⁾Deimos Space, located at ESOC, Germany

⁴⁾GMV, located at ESOC, Germany

(Received June 21st, 2017)

To support Rosetta navigation relative to the comet, the orbit determination subsystem was charged with the task of estimating a large number of auxiliary parameters such as the comet orbital and rotational states, its gravitational field and the comet-fixed coordinates of many landmarks. These estimations were initially performed over long trajectory arcs and were thus arduous to converge. Moreover, they were computationally intensive since the orbit determination filter is implemented with dense matrix operations. To prepare for the final phase of the mission, which would bring Rosetta closer to the comet than it had ever been, it was necessary to update and refine these auxiliary parameters estimates and, in particular, to significantly increase the number of navigation landmarks. To support this in an efficient manner, the filter was modified to use multiple shooting and to better handle sparsity in the observations equations. This paper discusses the parameter estimation techniques implemented for Rosetta orbit determination and how they were used in the last months of the mission. It also presents the results of this process concerning the comet kinematic and dynamic parameters and their evolution.

Key Words: SRIF, multi-arc orbit determination, Rosetta, small body navigation, gravitational field

Nomenclature

Lowercase bold symbols denote vectors. Uppercase bold symbols denote matrices. Upright symbols denote functions.

Examples

x	:	a scalar variable
\mathbf{v}	:	a column vector
\mathbf{M}	:	a matrix
\mathbf{h}	:	a vector-valued function

Additional notations

\mathbf{v}^T	:	the transpose of vector \mathbf{v} , a row vector
$\mathbf{M}^{-1}, \mathbf{M}^T$:	the inverse and the transpose of \mathbf{M}
\mathbf{M}^{-T}	:	the inverse transpose of matrix \mathbf{M}
$\text{diag}(\mathbf{M})$:	the diagonal matrix with the same diagonal as matrix \mathbf{M}
\mathbf{I}_n	:	the $n \times n$ identity matrix
$\mathbf{0}, \mathbf{0}_{n,m}$:	zero matrix, the $n \times m$ zero matrix
$\ \mathbf{v}\ $:	Euclidean norm of vector \mathbf{v}
$ x $:	absolute value of x
$\left[\begin{array}{c c} \mathbf{A} & \mathbf{b} \\ \hline \mathbf{C} & \mathbf{d} \end{array} \right]_{x_0}$:	Square Root Information Array (SRIA) for least squares problem $\min_x \ \mathbf{A}(\mathbf{x} - \mathbf{x}_0) - \mathbf{b}\ $
$\left[\begin{array}{c c} \mathbf{A} & \mathbf{b} \\ \hline \mathbf{C} & \mathbf{d} \end{array} \right]_{x_0} \oplus \left[\begin{array}{c c} \mathbf{C} & \mathbf{d} \\ \hline \mathbf{C} & \mathbf{d} \end{array} \right]_{x_1}$:	SRIA for least squares problem $\min_x (\ \mathbf{A}(\mathbf{x} - \mathbf{x}_0) - \mathbf{b}\ + \ \mathbf{C}(\mathbf{x} - \mathbf{x}_1) - \mathbf{d}\)$
$\left[\begin{array}{c c} \mathbf{A} & \mathbf{b} \\ \hline \mathbf{C} & \mathbf{d} \end{array} \right]_{x_0} \equiv \left[\begin{array}{c c} \mathbf{C} & \mathbf{d} \\ \hline \mathbf{C} & \mathbf{d} \end{array} \right]_{x_1}$:	equivalence of two SRIA
\mathbb{R}	:	the set of real numbers
$\forall \mathbf{x} \in \mathbb{R}^n$:	for all vectors \mathbf{x} in \mathbb{R}^n
δ	:	Dirac delta function
$\mathcal{E}(\cdot)$:	the expectation operator
\exp	:	the exponential function

1. Introduction

The ESA Rosetta spacecraft followed comet 67P/Churyumov-Gerasimenko around the Sun for two years from August 2014 to September 2016.¹⁾ The spacecraft was navigated using Earth-based radiometric tracking data (2-way range and Doppler) augmented with space-based optical navigation data (directions to landmarks). The orbit determination program was solving simultaneously for the spacecraft state and for the comet orbital and rotational states.²⁾ For routine planning, short observation intervals were used and the comet spin direction, its gravity field coefficients and the navigation landmark coordinates were kept fixed. In order to obtain good estimates of those parameters, long orbit determination arcs were used. Convergence was then not easy to achieve and it was usually necessary to preset the values of many dynamic parameters to the results of preliminary runs using e.g. shorter observation intervals. Since the filter was also using dense matrix operations, each iteration was taking a considerable amount of CPU time. During the last two months of the Rosetta mission, the spacecraft was to fly three-day eccentric orbits with low pericentres.³⁾ In preparation for this flyover phase, it was necessary to increase the surface density of navigation landmarks and to improve the knowledge of the comet gravitational field. For this purpose, more than ten thousand landmarks were identified on the comet. An orbit determination using multiple disjoint arcs and a decomposition in landmarks subsets, to make use of the sparsity of the landmark observable modelling problem, was performed to determine the gravitational field and the many landmark coordinates.

The flyover phase itself would provide important data for estimating the gravitational field. However because of the many

low pericentres, convergence of long observation interval orbit determinations would not be possible due to strong nonlinearities. A multi-arc approach was used instead. Matching constraints for the trajectories at arc boundaries were added as observation equations. The multiple shooting strategy not only made convergence easy, reducing the number of iterations, but also increased the sparsity of the problem making each iteration faster to compute. Multi-arc orbit determinations were run regularly during the final phase of the mission to update the gravitational field coefficients and the direction of the comet spin vector in inertial frame and in comet-fixed frame.

For navigation purposes, it was necessary to monitor the evolution of the comet dynamical parameters. In October 2014, orbit determination runs had already shown that the activity of the comet was modifying its rotation period. Later as the comet was approaching perihelion, significant changes were also observed in its inertial spin direction and its orbital elements. After perihelion, a change in the spin vector direction in body frame was measured.

Section 2. describes the techniques used in the Rosetta orbit determination filter. The estimation problem decomposition between local and global parameters and the multi-arc technique is explained in section 3.. Finally, section 4. presents the usage of those techniques in the last stages of the mission and discusses the observability of the 67P gravitational field as well as the observability and evolution of the comet's dynamical parameters during the two years Rosetta spent at the comet.

2. The Rosetta Orbit Determination Filter

This section explains the estimation problem and gives an overview of the methods implemented in the Rosetta orbit determination filter. This filter is used for all ESA deep space missions but some features (e.g. constraints, Levenberg-Marquardt method) were originally implemented to support Rosetta operations at comet 67P.

2.1. The estimation problem

We are given:

- An actual observation vector \mathbf{h}_{true} of dimension m .
- An observation model $\mathbf{h} : \mathbb{R}^n \rightarrow \mathbb{R}^m$, a function which given the parameter vector \mathbf{x} of dimension n computes the expected observation vector of dimension m .
- An initial guess for the parameter vector \mathbf{x}_0 .

The modelled observation vector is then: $\mathbf{h}_0 = \mathbf{h}(\mathbf{x}_0)$. The difference between the observed and modelled observation vector is the residual vector:

$$\mathbf{r}_0 = \mathbf{h}_{true} - \mathbf{h}_0 = \mathbf{h}_{true} - \mathbf{h}(\mathbf{x}_0) = \mathbf{r}(\mathbf{x}_0) \quad (1)$$

The residual function \mathbf{r} can be approximated in the vicinity of \mathbf{x}_0 by its linearisation:

$$\mathbf{r}(\mathbf{x}) = \mathbf{h}_{true} - \mathbf{h}(\mathbf{x}) \approx \mathbf{r}_0 - \mathbf{H}_0(\mathbf{x} - \mathbf{x}_0) \quad (2)$$

where \mathbf{H}_0 is the jacobian of \mathbf{h} at \mathbf{x}_0 , an $m \times n$ matrix:

$$\mathbf{H}_0 = \frac{\partial \mathbf{h}}{\partial \mathbf{x}}(\mathbf{x}_0) \quad (3)$$

We define $\tilde{\mathbf{r}}$:

$$\tilde{\mathbf{r}}(\mathbf{x}) = \mathbf{r}_0 - \mathbf{H}_0(\mathbf{x} - \mathbf{x}_0) \quad (4)$$

In the linear model assumption, a perfect fit would result in $\tilde{\mathbf{r}}(\mathbf{x}) = \mathbf{0}$. However, we normally have a heavily over-constrained system: $m \gg n$ and we choose \mathbf{x} to minimise the Euclidean norm of $\mathbf{W}\tilde{\mathbf{r}}(\mathbf{x})$ where \mathbf{W} is the residual weighting matrix:

$$\min_{\mathbf{x}} \|\mathbf{W}\tilde{\mathbf{r}}_0 - \mathbf{W}\mathbf{H}_0(\mathbf{x} - \mathbf{x}_0)\| \quad (5)$$

We will be using the following notation to represent this least squares problem:

$$\left[\mathbf{A} \mid \mathbf{b} \right]_{\mathbf{x}_0} \quad (6)$$

with:

$$\begin{aligned} \mathbf{A} &= \mathbf{W}\mathbf{H}_0 \\ \mathbf{b} &= \mathbf{W}\mathbf{r}_0 \end{aligned} \quad (7)$$

where each row of the system is an observation equation and each column of \mathbf{A} corresponds to a parameter.

2.2. Residual weighting matrix

The goal of the residual weighting is to obtain uncorrelated and uniformly weighted observation equations. For this purpose the $m \times m$ weighting matrix should be chosen as the inverse of a square root of the covariance matrix of the residual vector \mathbf{r}_0 :

$$\mathbf{W}^{-1}\mathbf{W}^{-T} = \mathcal{E}\left((\mathbf{r}_0 - \mathcal{E}(\mathbf{r}_0))(\mathbf{r}_0 - \mathcal{E}(\mathbf{r}_0))^T\right) \quad (8)$$

With this choice, the covariance matrix of the weighted residual vector \mathbf{b} is equal to the $m \times m$ identity matrix:

$$\mathcal{E}\left((\mathbf{b} - \mathcal{E}(\mathbf{b}))(\mathbf{b} - \mathcal{E}(\mathbf{b}))^T\right) = \mathbf{I}_m \quad (9)$$

The number of observations m is usually large and computing an $m \times m$ matrix square root is prohibitive unless we can take advantage of the sparsity of the correlations. In Rosetta orbit determination, we only assume correlations between disjoint pairs of observations (e.g. landmark x and y coordinates in camera plane) and thus we can decorrelate the observations by processing two rows of the observation matrix at a time.

In the absence of an experimental data collection or of a theoretical model, the variance and correlation of observations can be obtained from the statistics of the post-fit residuals provided that there is a large number of observations of the same type and taken in similar conditions. Ideally the post-fit residual mean should be zero. Post-fit residual biases are however frequent (at least on short time intervals) because of modelling errors. Since the post-fit covariance estimate is used as a measure of the precision of the solution, to account for modelling errors, observations should be weighted conservatively. Our usual approach is to target a weighted root mean square of the post-fit residual (not the standard deviation for robustness against biases) of about 0.5 for each data type (Doppler, range, landmark x and landmark y), sometimes using different weights for different time intervals (e.g. covering a ground station pass for weighting radiometric tracking).

Applying an effective weighting scheme is a key element in orbit determination. In the following sections, we assume that observations equations have been properly weighted.

2.3. The solution

We assume in this section that matrix A has rank n . The solution of $\left[A \mid b \right]_{x_0}$ can easily be shown to be given by the normal equation:

$$\Delta x_S = x_S - x_0 = (A^T A)^{-1} A^T b \quad (10)$$

The matrix $(A^T A)^{-1} A^T$ is the Moore-Penrose pseudo-inverse of A . The estimate for the covariance matrix of the solution vector is then:

$$C_S = (A^T A)^{-1} \quad (11)$$

(x_S, C_S) is the so-called filter solution.

However, methods which evaluate $A^T A$ to obtain the least squares solution are known to have poor stability and numerical accuracy. A method which avoids this computation is the Square Root Information Filter (SRIF).⁴⁾

2.4. The SRIF

If Q is an $m \times m$ orthogonal matrix ($Q^T Q = I_m$), we have:

$$\forall v \in \mathbb{R}^n, \|Av - b\| = \|Q(Av - b)\| = \|QA v - Qb\| \quad (12)$$

Hence the problem is equivalent to:

$$\left[QA \mid Qb \right] \quad (13)$$

The goal is to find Q such that:

$$QA = \begin{pmatrix} U \\ \mathbf{0}_{m-n,n} \end{pmatrix} \quad (14)$$

where U is an $n \times n$ upper triangular matrix.

Q can be generated by a sequence of elementary orthogonal transformations known as Householder reflectors.⁵⁾ The first Householder reflector is designed to zero out the last $m-1$ elements of column 1, the second to zero out the last $m-2$ elements of column 2 and so on. Reflector i acts only on the last $m-i+1$ rows of the system of equations and is designed using only the last $m-i+1$ elements of column i . With n householder reflectors, we obtain a triangular system.

Q does not need to be explicitly computed: the orthogonal Householder reflectors are applied in sequence to obtain:

$$\left[A \mid b \right] \equiv \left[\begin{array}{c|c} U & \begin{matrix} \tilde{b}_1 \\ \tilde{b}_2 \end{matrix} \\ \hline \mathbf{0}_{m-n,n} & \end{array} \right] \quad (15)$$

We have:

$$\forall v \in \mathbb{R}^n, \|Av - b\| = \|Uv - \tilde{b}_1\| + \|\tilde{b}_2\| \geq \|\tilde{b}_2\| \quad (16)$$

Thus the solution is given by:

$$\Delta x_S = x_S - x_0 = U^{-1} \tilde{b}_1 \quad (17)$$

and:

$$C_S = (U^T U)^{-1} = U^{-1} U^{-T} \quad (18)$$

The triangular system can be efficiently inverted to get Δx . U^{-1} and U^{-T} can also be computed efficiently. This algorithm is known as the Square Root Information Filter (SRIF).

The least squares objective is:

$$e^2 = \|\tilde{b}_2\|^2 = \|AAx_S - b\|^2 \quad (19)$$

Rows of zeros can be ignored:

$$\left[A \mid b \right] \equiv \left[\begin{array}{c|c} U & \tilde{b}_1 \\ \hline \mathbf{0}_{1,n} & \pm e \\ \mathbf{0}_{n-1,n} & \mathbf{0}_{n-1,1} \end{array} \right] \equiv \left[\begin{array}{c|c} U & \tilde{b}_1 \\ \hline \mathbf{0}_{1,n} & \pm e \end{array} \right] \quad (20)$$

Since we do not care about the least squares objective value, but only about the solution vector and its covariance matrix, we also have the following equivalence:

$$\left[A \mid b \right] \equiv \left[U \mid \tilde{b}_1 \right] \quad (21)$$

A and U are Square Root Information Arrays (SRIA) of the least squares problem. A given problem can be represented by many different square root information arrays, but the product:

$$\Lambda = A^T A = U^T U \quad (22)$$

is unique and is called the information matrix. Its inverse is the covariance of the solution vector.

In this paper we use the term SRIA to refer to the problem matrix A or U plus the right-hand side column vector b or \tilde{b}_1 (column which we consider as the last or $n+1$ column of the SRIA) plus the current value of the parameter vector x_0 . Hence we use the following notations:

$$\begin{aligned} \text{SRIA}_1 &= \left[A \mid b \right]_{x_0} \\ \text{SRIA}_2 &= \left[U \mid \tilde{b}_1 \right]_{x_0} \end{aligned} \quad (23)$$

and we have:

$$\begin{aligned} \text{SRIA}_1 &\neq \text{SRIA}_2 \\ \text{SRIA}_1 &\equiv \text{SRIA}_2 \end{aligned} \quad (24)$$

It is also easy to show that:

$$\left[A \mid b \right]_{x_0} \equiv \left[A \mid b + A(x_0 - x_1) \right]_{x_1} \quad (25)$$

2.5. Sequential estimation

The SRIF is well suited to sequential estimation. If we have a new set of observations $\left[C \mid d \right]$, the augmented system:

$$\left[\begin{array}{c|c} A & b \\ \hline C & d \end{array} \right] \quad (26)$$

is equivalent to:

$$\left[\begin{array}{c|c} U & \tilde{b}_1 \\ \hline C & d \end{array} \right] \quad (27)$$

No matrix inverse needs to be computed to update the SRIA. Additionally the intermediate systems need not be invertible and we can keep adding observations without computing an estimate until we get an invertible (and well conditioned) triangular system. Thus each scalar observation (row) can be processed and integrated into the upper triangular system as soon as it is generated avoiding the need for large matrix storage.

We use the following notation:

$$\left[A \mid b \right] \oplus \left[C \mid d \right] = \left[\begin{array}{c|c} A & b \\ \hline C & d \end{array} \right] \quad (28)$$

to represent the augmented system. Given SRIA_1 , SRIA_2 and SRIA_3 , three square root information arrays, we have the following relations:

$$(\text{SRIA}_1 \oplus \text{SRIA}_2) \oplus \text{SRIA}_3 = \text{SRIA}_1 \oplus (\text{SRIA}_2 \oplus \text{SRIA}_3) \quad (29)$$

$$\text{SRIA}_1 \oplus \text{SRIA}_2 \equiv \text{SRIA}_2 \oplus \text{SRIA}_1 \quad (30)$$

2.6. A priori information

A priori information can be crucial in making the problem well conditioned when some parameters are poorly observable. This information is usually in the form of an a priori parameter vector \mathbf{x}_a and an a priori covariance matrix \mathbf{C}_a or equivalently a square root information array. The a priori knowledge can be the solution of a previous determination. In that case no observations which were used to obtain that knowledge should be used again. The a priori covariance or square root information array needs to be mapped (section 2.10.) if the epochs for state parameters differ from those of the previous solution.

A SRIA for a priori information given by \mathbf{x}_a and \mathbf{C}_a is:

$$\left[\begin{array}{c|c} \mathbf{\Gamma}_a & \mathbf{0}_{n,1} \end{array} \right]_{\mathbf{x}_a} \quad (31)$$

where:

$$\mathbf{\Gamma}_a^T \mathbf{\Gamma}_a = \mathbf{C}_a^{-1} \quad (32)$$

$\mathbf{\Gamma}_a$ can be computed by factoring \mathbf{C}_a into $\mathbf{U}_a \mathbf{U}_a^T$ with \mathbf{U}_a upper triangular. Then $\mathbf{\Gamma}_a = \mathbf{U}_a^{-1}$ is also upper triangular.

Adding a priori information is analogous to adding observations to a SRIF:

$$\left[\begin{array}{c|c} \mathbf{A} & \mathbf{b} \end{array} \right]_{\mathbf{x}_0} \oplus \left[\begin{array}{c|c} \mathbf{\Gamma}_a & \mathbf{0}_{n,1} \end{array} \right]_{\mathbf{x}_a} \equiv \left[\begin{array}{c|c} \mathbf{A} & \mathbf{b} \\ \hline \mathbf{\Gamma}_a & \mathbf{\Gamma}_a(\mathbf{x}_a - \mathbf{x}_0) \end{array} \right]_{\mathbf{x}_0} \quad (33)$$

2.7. Constraints

One way to enforce algebraic constraints in a least squares fit is to reparametrize the problem by expressing the parameter vector in terms of a new parameter vector of lower dimension. Another method is to write the constraint as an observation equation: the ‘‘observed value’’ is zero and the observation model is such that the constraint is verified if and only if the modelled value is zero. With this method the constraint is not properly enforced, but by choosing a large enough weight for this observation we can control how strongly we want the constraint to be verified. However, a weight unnecessarily large should be avoided as it can lead to a system with a poor numerical condition.

The Rosetta orbit determination filter supports user input linear constraints between solve-for parameters (the coefficients are fixed for all iterations of the program). Internally, the constraints are treated as observation equations with user selected weight.

2.8. Process noise

Stochastic processes such as Solar Radiation Pressure (SRP) and Coma Drag cannot be accurately accounted for, but it is possible to model somewhat their variability in time by using different solve-for parameters for different time intervals. Let $p(t)$ be a stochastic process. For example, $p(t)$ could be the SRP model acceleration scale factor correction for time t :

$$SRP = (1 + bias + p(t))SRP_{nominal} \quad (34)$$

We discretize the process by defining a time-grid $(t_i), i = 1..n, t_i < t_{i+1}$ and:

$$P_i = p(t_i) \quad (35)$$

The scale factor applied in batch i is then $P_{bias} + P_i$. P_{bias} and $P_i, i = 1..n$ are $n + 1$ solve-for parameters.

It may be useful to constrain the solution by adding a priori information on the stochastic process. A frequent model

for stochastic processes is the following stochastic differential equation:

$$\frac{dp}{dt}(t) = -\frac{1}{\tau}p(t) + w(t) \quad (36)$$

where w is white zero-mean process noise with autocorrelation:

$$\mathcal{E}(w(t_1)w(t_2)) = \frac{2}{\tau}\sigma_p^2\delta(t_1, t_2) \quad (37)$$

where τ is the process autocorrelation time. p has steady state mean zero and variance σ_p^2 . The P_i are then exponentially correlated random variables:

$$\mathcal{E}(P_i P_j) = \exp\left(-\frac{|t_i - t_j|}{\tau}\right)\sigma_p^2 \quad (38)$$

This a priori information is given as a dense covariance matrix which is not suitable for the sequential constraint processing and parameter substitution that will be discussed in section 3.5.. However this information can be formulated in a sequential manner as the following set of linear observation equations:

$$\begin{aligned} P_1 &= 0, \text{ weight} = \frac{1}{\sigma_p} \\ P_{i+1} - \alpha_i P_i &= 0, \text{ weight} = \frac{1}{\sigma_p \sqrt{1 - \alpha_i^2}} \end{aligned} \quad (39)$$

with:

$$\alpha_i = \exp\left(-\frac{t_{i+1} - t_i}{\tau}\right) \quad (40)$$

Those equations are equivalent, from the least squares point of view, to the covariance matrix of Eq. (38) including the diagonal terms. Similar sequential equations, can also be formulated for random walk processes (the integral of a white-noise process) and ‘‘exponentially correlated’’ random walk (the integral of an exponentially correlated process). In the last case, these equations relate three consecutive batch parameters.

2.9. Consider parameters

In interplanetary orbit determination, many uncertain parameters are poorly observable. Such parameters could be ground station coordinates or Earth orientation parameters. Their uncertainty has to be taken into account in the computation of the post-fit covariance of the parameter vector. They cannot in general be solved-for because the combination of their poor observability with simplistic models could lead to solution biases and over-confidence in the solution (post-fit covariance too optimistic). In that case, it is possible to decompose the parameter vector into solve-for vector \mathbf{x}^S of dimension k and a consider vector \mathbf{x}^C of dimension $n - k$. In the following discussion we assume that the parameter vector ordering is such that $\mathbf{x} = [\mathbf{x}^S, \mathbf{x}^C]$. If this is not the case, the parameter vector and the columns of the matrix \mathbf{A} in the left hand side of the SRIA can be re-ordered accordingly. The SRIA is decomposed into:

$$\left[\begin{array}{c|c|c} \mathbf{A}^S & \mathbf{A}^C & \mathbf{b} \end{array} \right]_{[\mathbf{x}_0^S, \mathbf{x}_0^C]} \quad (41)$$

where \mathbf{A}^S has k columns and \mathbf{A}^C has $n - k$ columns. \mathbf{A} does not need to be full rank, but \mathbf{A}^S does. We can perform k householder transformations to obtain an equivalent SRIA:

$$\left[\begin{array}{c|c|c} \mathbf{U} & \tilde{\mathbf{A}}_1^C & \tilde{\mathbf{b}}_1 \\ \mathbf{0} & \tilde{\mathbf{A}}_2^C & \tilde{\mathbf{b}}_2 \end{array} \right]_{[\mathbf{x}_0^S, \mathbf{x}_0^C]} \quad (42)$$

with U upper triangular.

For a fixed given value of x^C , the optimal solution is:

$$x^S - x_0^S = U^{-1}\tilde{b}_1 - U^{-1}\tilde{A}_2^C(x^C - x_0^C) \quad (43)$$

The matrix:

$$S = -U^{-1}\tilde{A}_2^C \quad (44)$$

is the sensitivity matrix of the solve-for parameters to the consider parameters.

The consider parameter vector is not updated. Hence the solution is given by:

$$\Delta x_S^S = x_S^S - x_0^S = U^{-1}\tilde{b}_1 \quad (45)$$

The solution vector would be the same if the consider parameters had been ignored in the fit. In particular, it is independent of the uncertainties in the consider parameters.

Given a guess for the consider parameters uncertainty in the form of a covariance matrix:

$$C_0^C = \mathcal{E}((x^C - x_0^C)(x^C - x_0^C)^T) \quad (46)$$

we can compute the covariance estimate of the solve-for parameters:

$$C_C = C_F + C_+ \quad (47)$$

$$C_F = U^{-1}U^{-T} \quad (48)$$

$$C_+ = SC_0^CS^T \quad (49)$$

C_C is called the consider covariance, C_F the filter covariance. C_+ is the contribution of the consider parameters to the covariance of the solve-for parameters.

The consider covariance is always “larger” than (or equal to) the filter covariance. Consider parameters should be used with care since their effects are not always intuitive.⁶⁾ While the filter covariance can only decrease with new observations, the consider covariance may increase.

2.10. Mapping

A change in the parameter vector x can be mapped into a change in a state y at any given time t (under assumption of linearity of the dynamic models):

$$y(t) - y_0(t) = \Phi_0(t)(x - x_0) \quad (50)$$

where:

- y_0 is the integrated trajectory for parameter vector value x_0 .
- Φ_0 is the corresponding state mapping matrix “trajectory” obtained from integrating the variational equations.

As explained in section 2.1 of Ref. 2), for Rosetta orbit determination, the comet attitude, comet orbit and spacecraft orbit are integrated separately. The parameters in x which encode those states at a certain epoch (possibly different epochs for all three trajectories) are called state parameters. The mapping of the parameter vector x from a set of three epochs to another set of three epochs consist in replacing the state parameters by the encoding of the corresponding state vectors at the new epochs. The new state vector x^{map} is then related to x by:

$$x^{map} - x_0^{map} = \Sigma(x - x_0) \quad (51)$$

where Σ is the parameter transition matrix for the new set of epochs. This matrix is obtained from the transition matrices of the three trajectories at their respective new epochs and the quaternion parameter encoding matrix $S(q_0^{map})$ described in section 4.3 of Ref. 2) where q_0^{map} is the attitude quaternion at the new attitude epoch. Given the SRIA $[A \mid b]_{x_0}$ for parameter vector x , the equivalent SRIA for parameter x^{map} is then:

$$[A\Sigma^{-1} \mid b]_{x_0^{map}} \quad (52)$$

and the mapping of the covariance matrix C of x is:

$$C^{map} = \Sigma C \Sigma^T \quad (53)$$

The non-state parameters values and covariance matrix are unchanged by the mapping (except for the state parameters, Σ is the identity) but their cross-covariance with the state parameters is modified.

Assuming that no state parameter is treated as a consider parameter, it is easy to show that the mapping of the consider covariance equals the consider covariance of the mapped SRIA.

2.11. Dealing with problem nonlinearity

The orbit determination problem is nonlinear, so the solution needs to be iterated. Given a solution vector x_n , the problem is linearized again in the vicinity of x_n to obtain a new linear system which is solved to get a new solution x_{n+1} until convergence is achieved. When the initial guess is too far from the solution, convergence may be difficult. One possible remedy is to use the Levenberg method or damped least squares:

$$(A^T A + \lambda I_n) \Delta x_S = A^T b \quad (54)$$

or its regularized version the Levenberg-Marquardt method:

$$(A^T A + \lambda \text{diag}(A^T A)) \Delta x_S = A^T b \quad (55)$$

where $\lambda \geq 0$ is the damping parameter. When $\lambda = 0$, the Levenberg method is the same as the least squares method. When λ is large, this method approaches the gradient descent method with a very small step. Starting with a large value of the damping parameter can help to avoid overshooting by far the solution in the presence of nonlinearities. As the estimate approaches the solution, the damping parameter can be reduced. Choosing a good value for the initial damping parameter and a strategy for its update between iterations is, however, not trivial and some heuristic and theoretical arguments have been proposed in the literature.

The Levenberg and Levenberg-Marquardt methods can be implemented in the SRIF. The SRIF formulation for the Levenberg Marquardt version of $[A \mid b]_{x_0}$ is:

$$[A \mid b]_{x_0} \oplus [\sqrt{\lambda \text{diag}(A^T A)} \mid \mathbf{0}_{n,1}]_{x_0} \quad (56)$$

which is computed more efficiently after the SRIA $[A \mid b]_{x_0}$ has first been made upper triangular.

The Levenberg-Marquardt method is more robust than the normal least squares method but is still a local solution method.

When the orbit determination arc becomes too long (encompassing many orbits), small errors in dynamic parameters (including state parameters at epoch) can lead to very large state

errors after some time (many revolutions). For a long orbit determination arc, it is usually required to start with very good estimates for the dynamic parameters (e.g. epoch state, manoeuvres performances, gravitational field, drag and solar radiation pressure coefficients). To obtain these estimates, an easy method is to define nested intervals where the last interval is the desired interval for the long arc determination and to perform a sequence of orbit determinations starting with an arc reduced to the first interval and ending with the final interval, using, at each step, the solution of the previous step in the new initial guess. This method had been used for Rosetta orbit determination. However it has several drawbacks:

- It is a cumbersome and rather inefficient process, requiring many iterations.
- The state mapping matrix may be poorly conditioned after long propagation intervals.
- Due to the large number of dynamic parameters (such as wheel desaturation manoeuvres components) that can modify the state between estimation epoch and observation participation time, the problem matrix is usually large and not sparse in the columns corresponding to the dynamic parameters.

These issues can be addressed by the multi-arc orbit determination method which is described in the next section.

3. Local-global parameters decomposition and multi-arc orbit determination

3.1. Local-global parameter decomposition

First, we consider a problem with two sets of observation equations. The decomposition between the observation sets does not need to be a decomposition in time intervals/observation arcs. Each set applies to a different subset of parameters but these subsets intersect. We call the overlapping subset the set of global parameters. The observations of set 1 are given in term of the global parameters x^G plus additional parameters x^{L1} which we call local parameters of set 1. Similarly the observations of set 2 are given in terms of the global parameters and the local parameters of set 2, x^{L2} . We assume that the

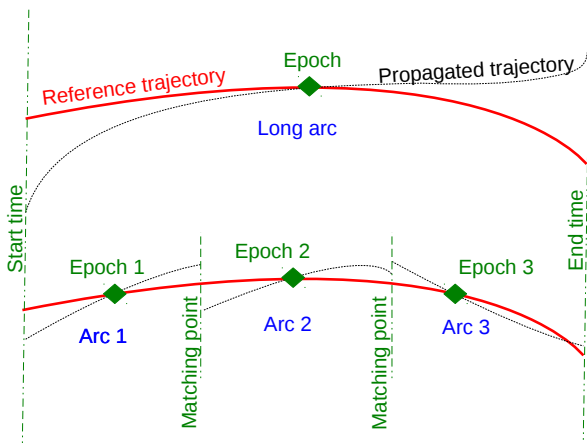


Fig. 1. Illustration of the multi-arc method (bottom) compared to single arc (top).

parameter vector ordering for set 1 equations is $[x^{L1}, x^G]$ and the for set 2 equations is $[x^{L2}, x^G]$: this can be achieved by a permutation of the rows of the matrices. The SRIA for set 1 and set 2 observations are given:

$$\left[\begin{array}{c|c|c} x^{L1} & x^G & \\ \hline A_{L1} & A_{G1} & b_1 \end{array} \right]_{[x_0^{L1}, x_{01}^G]} \quad (57)$$

$$\left[\begin{array}{c|c|c} x^{L2} & x^G & \\ \hline A_{L2} & A_{G2} & b_2 \end{array} \right]_{[x_0^{L2}, x_{02}^G]} \quad (58)$$

First, to prepare for the substitution of the local parameters, we make the SRIA upper triangular in the columns of the local parameters by applying the adequate Householder reflections:

$$\left[\begin{array}{c|c|c} x^{L1} & x^G & \\ \hline U_{L1} & \tilde{A}_{G1} & \tilde{b}_1 \\ \hline 0 & \hat{A}_{G1} & \hat{b}_1 \end{array} \right]_{[x_0^{L1}, x_{01}^G]} \quad (59)$$

$$\left[\begin{array}{c|c|c} x^{L2} & x^G & \\ \hline U_{L2} & \tilde{A}_{G2} & \tilde{b}_2 \\ \hline 0 & \hat{A}_{G2} & \hat{b}_2 \end{array} \right]_{[x_0^{L2}, x_{02}^G]} \quad (60)$$

It is not necessary to perform the full matrix triangularization, but it can be convenient: if \tilde{A}_{G1} and \tilde{A}_{G2} are upper triangular matrices then many rows of zeros can be dropped from the matrices. Combining the two sets of equations, we obtain the following SRIA:

$$\left[\begin{array}{c|c|c|c} x^{L1} & x^{L2} & x^G & \\ \hline U_{L1} & 0 & \tilde{A}_{G1} & \tilde{b}_1 \\ \hline 0 & U_{L2} & \tilde{A}_{G2} & \tilde{b}_2 + \tilde{A}_{G2}(x_{02}^G - x_{01}^G) \\ \hline 0 & 0 & \hat{A}_{G1} & \hat{b}_1 \\ \hline 0 & 0 & \hat{A}_{G2} & \hat{b}_2 + \hat{A}_{G2}(x_{02}^G - x_{01}^G) \end{array} \right]_{[x_0^{L1}, x_0^{L2}, x_{01}^G]} \quad (61)$$

where the right-hand side has been corrected for a potential difference in global parameter values between the two sets of equations. At this point, we can add additional equations (rows) that depend on global parameters only. Assuming that the system has full rank, it is then obvious that the global parameter solution is obtained from the following SRIA:

$$\left[\begin{array}{c|c} x^G & \\ \hline \hat{A}_{G1} & \hat{b}_1 \\ \hline \hat{A}_{G2} & \hat{b}_2 + \hat{A}_{G2}(x_{02}^G - x_{01}^G) \end{array} \right]_{x_{01}^G} \quad (62)$$

and that the local parameter solution (x_S^{Li}, C_{Li}) for arc i , $i = 1, 2$ can be determined from the global parameter solution (x_S^G, C_G) by back substitution:

$$\begin{aligned} x_S^{Li} - x_0^{Li} &= U_{Li}^{-1} \tilde{b}_i + S_i (x_S^G - x_{0i}^G) \\ C_{Li} &= U_{Li}^{-1} U_{Li}^{-T} + S_i C_G S_i^T \end{aligned} \quad (63)$$

where S_i is the sensitivity matrix of arc i local parameters to global parameters:

$$S_i = -U_{Li}^{-1} \tilde{A}_{Gi} \quad (64)$$

The estimate for the cross covariance between local parameters of set i and global parameters is given by $S_i C_G$ and the one for the cross covariance between local parameters of set 1 and local parameters of set 2 is given by $S_1 C_G S_2^T$.

The important point to note here is that it is not needed to build the full matrix of Eq. (61). Instead from Eq. (57) and Eq. (58), we perform triangularization by application of an orthogonal transformation to obtain Eq. (59) and Eq. (60) from which we build Eq. (62) where local parameters are factored out. We then solve for the global parameters. Finally using the global solution and again Eq. (59) and Eq. (60) we obtain the local solutions per Eq. (63). Thanks to this, even when using dense matrix operations, we are making use of the sparsity of the problem.

This technique can be applied to more than two observations sets. In that case, the global parameters are not defined by the intersection of the parameter vectors of all sets but by the set of parameters appearing at least in two observations sets. For a global parameter not appearing in a particular observation set, a zero column is then inserted in the rows of that observation set when building the SRIA for the global parameters (Eq. (62)).

A local parameter can only be factored out after all observations depending on that parameter have been processed. Hence it is important that all the a priori information concerning local parameters are processed before building Eq. (59) and Eq. (60). A priori information for global parameters can be added at a later stage in Eq. (62). If however it is processed in an earlier stage, it is important to make sure that it is not added to the equations of several sets as it would then weigh more than intended.

Consider parameters cannot be factored out and have to be treated as global parameters (even when they appear in a single observation set!). The consider solution for the global parameters is obtained from the global parameters SRIA (Eq (62)) by separating the global parameter vector in solve-for and consider parameters using the technique described in section 2.9.. Then, the consider (resp. filter) solution for the local parameters is simply given by Eq. (63) with (x_S^G, C_G) the consider (resp. filter) global solution.

Even with few or no local parameters that can be factored out, the technique may lead to significant gain when using dense matrix operations when the number of observations per set is large and the number of parameters per set is small compared to the total number of parameters. This is because processing observations into the SRIA takes a lot of CPU time and a huge gain is obtained when the number of parameters per SRIA is small. The merger of the SRIA is also fast since there are no more rows than parameters per SRIA (as long as the triangularization is performed on all columns).

3.2. Application of local-global decomposition to landmark coordinates estimation

For Rosetta navigation, more than 10000 landmarks were defined on the comet. The full observation matrix would then have more than 30000 columns. But it is a very sparse matrix since each landmark observation depends on the three coordinates of only one landmark.

If we group the observations per landmark and build a separate SRIA for each landmark, then each of those SRIA uses only three landmark coordinates parameters. If we then select those three parameters as the local parameters, we can use the method described in section 3.1. to solve for all landmarks while never having to deal with more than three landmarks coordinates parameters at a time. The global parameters in that case would be

dynamic parameters and other observation parameters (e.g. image biases). Other observations types (e.g. radiometric) could be handled by yet another SRIA, where the local parameters would be the corresponding observation parameters (e.g. range biases per pass) except for those that are treated as consider parameters.

This method works fine as long as we are not interested in camera biases per image. One image usually contains several observations of distinct landmarks but there are usually many more images than landmarks, in a large enough observation arc. If the image biases are to be treated as consider parameters, then they have to be treated as global parameters and cannot be factored out. If however, they are to be treated as solve-for parameters, then it is more efficient to separate observations per image and to treat the image biases as local parameters. Then, given that each particular landmark can be in many images, landmark coordinates have to be treated as global parameters and cannot be substituted.

3.3. Multiple shooting method

Propagating orbits over long time intervals can cause a divergence of the filter. To handle better the problem nonlinearity, the multiple shooting (or multi-arc) technique can be used. Figure 1 illustrates this method. It consists in separating the problem in several time intervals (arcs) and performing one propagation per interval starting from a reference trajectory at an epoch inside that time interval. The reference trajectory should be close enough to the actual trajectory. Thus inclusion of additional arcs may require a trajectory update from the solution of previous arcs. It may then seem that the process is not much better than the iterative long arc solution technique described in section 2.11.. However, there is an important difference. After a long arc is converged, a change in the dynamic model may require to restart the iterative process to solve for the dynamic parameters since a small change in the dynamics may cause a large propagation error at the boundaries of the arc, while when using a multi-arc technique this is not needed: any reference trajectory that is close enough to the actual trajectory will most likely allow the multi-arc to convergence very rapidly to the new solution after changing the dynamic model. Thus, many dynamic models may be tested efficiently. Additionally, the multi-arc technique has the advantage of a more sparse observation matrix (observations depend on fewer dynamic parameters) and a better conditioned system (state mapping matrix may be badly conditioned for large propagation interval).

The arcs usually do not overlap, but if they do any observation that fall into two or more arcs should only be processed in a single arc SRIA. So that the multi-arc method gives a solution consistent to the single arc solution, strict (heavily weighted) matching constraints should be applied between consecutive arcs. However, in case no matching constraints are applied, dynamic parameters (including initial state vectors) of each arc can be treated as local parameters and be factored out as described in section 3.1..

3.4. Matching constraints

Given two consecutive arcs i and $i + 1$, with matching point at $t_i^{match} = t_i^{end} = t_{i+1}^{start}$, the state \mathbf{y}_i^{end} (resp. \mathbf{y}_{i+1}^{start}) at the matching point for arc i (resp for arc $i + 1$) is approximated as an affine

function of the dynamic parameters:

$$\begin{aligned} \mathbf{y}_i^{end} &\approx \mathbf{y}_i^0(t_i^{match}) + \Phi_i^0(t_i^{match})(\mathbf{x}_i - \mathbf{x}_i^0) \\ \mathbf{y}_{i+1}^{start} &\approx \mathbf{y}_{i+1}^0(t_i^{match}) + \Phi_{i+1}^0(t_i^{match})(\mathbf{x}_{i+1} - \mathbf{x}_{i+1}^0) \end{aligned} \quad (65)$$

where:

- \mathbf{x}_i is the vector of dynamic parameter for arc i (some parameters may be common to both arcs).
- \mathbf{y}_i^0 is the propagated trajectory for arc i assuming the values of dynamic parameters \mathbf{x}_i^0 .
- Φ_i^0 is the associated state mapping matrix function.

If the matching time has to be estimated (this can be useful if the dynamic model changes at the matching point), the following equations should be used instead:

$$\begin{aligned} \mathbf{y}_i^{end} &\approx \mathbf{y}_i^0(t_i^{match0}) + \Phi_i^0(t_i^{match0})(\mathbf{x}_i - \mathbf{x}_i^0) \\ &\quad + \frac{d\mathbf{y}_i^0}{dt}(t_i^{match} - t_i^{match0}) \\ \mathbf{y}_{i+1}^{start} &\approx \mathbf{y}_{i+1}^0(t_i^{match0}) + \Phi_{i+1}^0(t_i^{match0})(\mathbf{x}_{i+1} - \mathbf{x}_{i+1}^0) \\ &\quad + \frac{d\mathbf{y}_{i+1}^0}{dt}(t_i^{match} - t_i^{match0}) \end{aligned} \quad (66)$$

where t_i^{match} is the parameter for the matching point time with current value t_i^{match0} .

The matching constraint is usually of the form:

$$\mathbf{f}(\mathbf{y}_i^{end}, \mathbf{y}_{i+1}^{start}) = \mathbf{0} \quad (67)$$

As explained in section 2.7., this constraint can be implemented as observation equations with observation model given by the function \mathbf{f} and observed value the vector $\mathbf{0}$. For the matching of the spacecraft relative (cometocentric) states, the model \mathbf{f} can be chosen as the difference between the vectors: $\mathbf{f}(\mathbf{y}_i^{end}, \mathbf{y}_{i+1}^{start}) = \mathbf{y}_i^{end} - \mathbf{y}_{i+1}^{start}$ leading to 6 equations. The same function can be chosen for the matching of the comet heliocentric states. However a different weighting matrix should probably be chosen for the spacecraft and the comet constraint. The matching constraint can also be used to implement a discontinuity, such as a manoeuvre at the matching point, by adding an offset to the state difference, in which case the weighting matrix should be adjusted so that the manoeuvre misperformance is reflected in the constraint residuals: in the case of a manoeuvre the weighting matrix \mathbf{W} of the constraint should be such that if the manoeuvre components were estimated dynamic parameters their a priori covariance would be set to $\mathbf{W}^{-1}\mathbf{W}^{-T}$.

For the matching of the comet attitude states, care should be taken when computing the attitude quaternion difference that both quaternions are less than 90 degrees apart on the 4-dimensional hypersphere, otherwise the quaternions should be added instead. Alternatively, the angle of the rotation between the two quaternions can also be used to define a constraint.

The matching constraints can be relaxed (small weight) to absorb dynamic mismodelling: this is particularly useful for the comet orbit reconstruction due to the usage of a dynamic model with little freedom and a poor or non-existent modelling of the non gravitational forces.

3.5. Multi-arc and local-global decomposition

When using matching constraints, it is not possible to substitute the dynamic parameters in each arcs individual SRIA before combining the SRIAs. However when equations which relate parameters from two arcs apply only to two consecutive arcs (sequential constraint), it is possible to perform an efficient multi-stage/nested decomposition of the problem:

1. Build the SRIA for each arc $\mathbf{SRIA}_i, i = 1..n$.
2. Set $i = 1$ and $\mathbf{SRIA}_i^* = \mathbf{SRIA}_i$.
3. Merge \mathbf{SRIA}_i^* and \mathbf{SRIA}_{i+1} taking care to appropriately reorder the columns and possibly adjust the right-hand side for differences in parameter values.
4. Add state matching constraints and possibly sequential equations relating other dynamic and observation parameters (SRP scale factor, camera image bias per arc/per image, see also section 2.8.) between arcs i and $i + 1$ to get $\mathbf{SRIA}_{i,i+1}$.
5. If $i + 1 = n$, go to step 8.
6. At this point solve-for dynamic parameters and solve-for local observation parameters of arc i (range biases per pass, image biases per arc/per image) can be substituted: reorder $\mathbf{SRIA}_{i,i+1}$ accordingly and apply the SRIF triangulation algorithm. $\mathbf{SRIA}_{i,i+1}^*$ is then the extracted SRIA for the ‘‘current global’’ parameters (lower right block of SRIA), \mathbf{x}_i^0 is the current local parameter solution and \mathbf{S}_i is the sensitivity of the local parameters to the global parameters.
7. Set $i = i + 1$ and go to step 3.
8. Solve $\mathbf{SRIA}_{n-1,n}$ taking into account possible consider parameters to get solution \mathbf{x}_{n-1} for the global parameters and the ‘‘local’’ parameters of the last two arcs.
9. Set $i = n - 1$
10. If $i = 1$, finish.
11. Using $\mathbf{x}_{i-1}^0, \mathbf{S}_{i-1}$ and \mathbf{x}_i compute solution \mathbf{x}_{i-1} for ‘‘local’’ parameters of arc $i - 1$ to n and global parameters (similar to Kalman smoothing).
12. Set $i = i - 1$ and go to step 10.

The final solution is obtained from a chain of back substitution (steps 9-12).

If however it is intended to use the method described in section 3.2. to handle landmarks one by one, then the algorithm described above cannot be used and all dynamic parameters have to be treated as global parameters.

3.6. Implementation

The Rosetta orbit determination filter is part of an all in one legacy FORTRAN program which does all the orbit determination tasks in the following sequence:

1. Propagate trajectories with variational equations.
2. Model observations and compute residuals.
3. Check residuals for convergence and if converged go to step 8.
4. Merge observations equations into SRIA.
5. Add a priori parameter information and linear constraints equations.
6. Solve SRIA and update parameters.
7. Go to step 1.
8. Compute filter and consider covariance.

It uses dense matrix operations and does not handle local-global parameter decomposition, arc or observation dataset decomposition, multiple shooting or nonlinear constraints (such as trajectory matching constraints) and it cannot make use of several CPUs. Those features were implemented in python modules. However the dynamic and observation modelling are still performed by the same FORTRAN program. A python routine takes care of configuring and calling the FORTRAN program in such a way that the program stops at steps 4 or 5. Then, python routines read the output trajectories and SRIA, add matching constraints, solve the system and builds the inputs for the next iteration using methods described in this section. Most of the mathematical operations are implemented using numpy and scipy libraries,⁷⁾ while the multiprocessing library⁸⁾ is used to launch several instances (one per arc/dataset) of the FORTRAN modelling program simultaneously on different CPUs.

4. Operational experience

Figure 2 gives an overview of the trajectory flown in the last 7 months of the Rosetta mission. The solar phase angle is the angle between the comet centre to spacecraft vector and the comet to sun vector. Low phase angles provide good target illumination. In the assumption of a radial flow of gas from the comet centre, dynamic perturbations are smaller in the terminator plane (90 degrees solar phase angle), since in that case the solar panels are edge on to the flow.

In 2015, around comet perihelion, the spacecraft had to fly far (up to a few hundreds of kilometres) from the comet. In March 2016, it was brought down to about 12 kilometres from the comet centre in the terminator plane. Afterwards, it was sent into a night-side excursion. In May, it was back in the terminator plane, flying closer orbits down to 7-kilometre radius circular. In June, Rosetta was flying circular orbits 30 kilometres from the comet centre inclined 45 degrees from the terminator in the day side. Those orbits were useful for building new maps of the comet and compiling a large database of landmarks in preparation for the last two months of the mission. This phase was called Mapping Phase.

The End of Mission plan,³⁾ was to bring the spacecraft in elliptical orbits with a period of three days at the end of July and then to progressively reduce the pericentre altitude while maintaining the orbital period. Finally at the end of September, the spacecraft was to be navigated towards a soft touchdown on the surface of the comet and be passivated. For trajectory control during the three-day elliptical orbit phase, called flyover phase, two manoeuvre slots were available per orbit: a pre- and a post-pericentre slot. Commands for trajectory control, attitude guidance and navigation images were uploaded at every apocentre. Navigation images were taken regularly targeting illuminated areas on the comet. Since the guidance was commanded relative to an inertial reference based on the predicted orbit, large pointing errors were expected around pericentres. This, combined with the small size of the imaged comet surface at such close distances, would have resulted in images with few or no landmark observations. Hence to support accurate navigation during this phase, the number of navigation landmarks was increased from a thousand to more than ten thousand based on

data acquired during the first half of 2016.

4.1. Preparing for end of mission

4.1.1. Landmark database

The optical navigation group,⁹⁾ produced half a million observations of more than 10000 landmarks in more than 3600 images taken between February 24 and July 12, 2016. The orbit determination group was tasked with the accurate determination of the body-fixed coordinates of those landmarks. For this purpose, an orbit determination process with a very large number of auxiliary parameters was run considering simultaneously three arcs that are highlighted in Fig. 2:

- **Arc 1:** The orange region covering February 24 to March 23 in the terminator plane with cometocentric distance down to 12 kilometres.
- **Arc 2:** The green region covering April 19 to May 28 mostly in the terminator plane with cometocentric distance down to 7 kilometres.
- **Arc 3:** The blue region covering May 29 to June 21, including the Mapping phase with cometocentric distance of about 30 kilometres and tilted 45 degrees with respect to the terminator plane.

This orbit determination was to provide a combined solution for the comet rotational parameters, the comet gravitational field and the landmark coordinates. Ideally as discussed in section 3.2., the observations should be grouped and processed per landmark. However, because the legacy FORTRAN modelling program can only generate observation equations with respect to dynamic parameters by re-propagating the associated trajectories and variational equations, this would have been inefficient. Instead, observations were grouped per landmark sets of about 800 landmarks. Moreover, we did not need to estimate all landmarks positions for our combined solution, but only a subset of the most observed landmarks providing a sufficient comet surface coverage. A first guess for the coordinates of all landmarks was obtained rapidly by fixing the trajectories (comet attitude, spacecraft relative orbit) to their reconstructions from the operational orbit determination. The selection of the landmarks for the combined solution was performed according to the following recipe:

1. Find most observed landmark not yet considered.
2. If this landmark is observed 10 times or less, finish.
3. If this landmark is not within 100 meters of an already selected landmark (according to preliminary coordinates solution), select this landmark.
4. Go to step 1.

This process selected 2438 landmarks that we distributed evenly (in number of landmarks and in number of observations) between three sets A, B and C.

On each arc, four runs of the FORTRAN modelling programs were performed per iteration: one for each landmark set plus one for the set of radiometric tracking data (set R). The estimation filter processing was performed according to the following multi-stage decomposition:

- Get the modelling program SRIA output for each combination of arc (1,2 or 3) and set (A, B, C and R): SRIA(arc,set)
- For all three SRIA(arc,R) perform a local-global decomposition selecting as local parameter the range biases per

- pass after processing their a priori information.
- For a given set merge the SRIA for all three arcs to obtain SRIA(set) after factoring out the range biases.
- For set=A,B and C, perform a local global decomposition of SRIA(set) selecting as local parameter the landmark coordinates.
- Merge all four SRIA(set) after factoring out the landmark coordinates.
- Add a priori information about global parameters (dynamic parameters, camera biases...).
- Add matching constraints: in most runs the only trajectory constraint that was used between the three arcs concerns the comet spin direction.
- Solve the global system taking into account consider parameters.
- Back-substitute in SRIA(set) to obtain local parameter solutions: the landmark coordinates.
- Back-substitute in SRIA(arc,set) to obtain local parameter solutions: the range biases.

The solution is iterated until convergence. Because each of the three arcs were rather long, they were first pre-converged separately. Parameters common to all arcs had then different first iteration values in each arc. This was fixed by the filter after the first update.

Several runs were performed to assess different models and constraints. In each run, 11104 two-way range observations, 13629 two-way Doppler observations, 143047 landmark observations and 2 Delta-DOR observations from two baselines were processed. The number of estimated parameters varied between 8000 and more than 10000 depending on the run (runs estimating camera pointing biases per comet imaging sequence had more parameters). Due to software limitations in maximum number of observations and maximum number of parameters, this estimation problem could not have been solved in a run of the legacy Rosetta orbit determination program.

Landmark observations were deweighted significantly from their usual weight, leading to small post-fit normalised residuals RMS. This was to balance the relative weight of optical to radiometric observations given the increase in the number of landmark observations and to counter the effect of not modelling the correlations between landmark observations (especially the ones in the same images).

Once the solution for the selected 2438 landmarks was obtained, the other landmark coordinates were solved in an estimation process in which the trajectories and other parameters were fixed to the results of the combined solution.

4.1.2. Comet gravity and attitude motion

In addition to the landmark coordinates, an important expected result of the multi-arc and multi-set orbit determination described in the previous section, was the comet gravitational field and pole direction. The estimates for the comet mass, gravitational field coefficients, centre of mass and spin vector direction in body-fixed frame had not been updated since the preparations for Philae landing.²⁾ The comet rotation period had evolved significantly during the time Rosetta spent at the comet and the spin phase, rate and rate rate estimates were updated in routine orbit determinations. The estimate for the spin vector direction in inertial frame had been updated less frequently

using long arc orbit determination solutions.

The solution for the centre of mass position and the pole direction in body-fixed frame were significantly different from their previous estimates (5 meters along the spin direction and 60 millidegrees). Throughout the mission, The body fixed frame was defined by the landmark coordinates.²⁾ Although the landmark coordinates estimates could be revised to take into account new observations and possible re-modelling of the comet surface after perihelion, the definition of the frame implied that there should no net rotation and translation between two landmark coordinates solutions. The frame had originally been conveniently chosen such that the centre of mass was at the origin and the spin direction was aligned with the canonical Z axis. With the new estimates, these two assumptions would not hold anymore.

In routine orbit determination, the spin direction in body frame and inertial frame was poorly observable and was enforced by parametrization, but, without the assumption of the spin vector being aligned to a canonical frame axis, this was not possible anymore with our model. Using a different frame definition for the routine orbit determination setup was considered but was ultimately decided against since this would have required the post-processing of the resulting comet orbit, comet attitude and any new landmarks coordinates before publishing them to external parties. Instead four scalar linear constraints equations were added to the routine setup and heavily weighted to enforce the spin direction in inertial frame and body frame to match the combined solution results. Similarly the offset of the centre of mass was modelled by a non-zero gravitational field coefficient of degree one and order 0: C_{10} . Thus the comet centre was not anymore its centre of mass, but the error this was causing in the comet orbit propagation was deemed negligible.

The combined solution for the comet attitude, landmark coordinates and gravitational field coefficients was thus rotated and translated back to the original frame for use in the routine orbit determination setup. There was however one exception: the newly determined spin axis was passing about 40 centimetres from the original frame origin and this was something our software and other parties involved in Rosetta operations could not cope with. Hence the new operational frame was not exactly the original frame but was different by a translation of about 40 centimetres.

4.2. Multi-arc runs during the last months

To monitor the evolution of the comet dynamic parameters and improve the gravitational field coefficient estimates, a multi-arc orbit determination was set-up for the end of mission phase and was run in parallel to the routine orbit determination. As Rosetta was flying very close to the comet at that time, long arc orbit determinations would have been practically impossible to converge. But the multi-arc filter was accomplishing this task very easily.

Each three-day eccentric orbit was defining an arc. Additional arcs were included prior to the flyover phase: In particular five arcs were defined between May 11 and May 28. Low altitude passages above a few comet regions during the last phase of the mission could negatively impact the estimates of the overall gravitational field. Thus the observation residuals in the May arcs were used to assess this possible degradation and to provide a source of global information on the comet gravity.

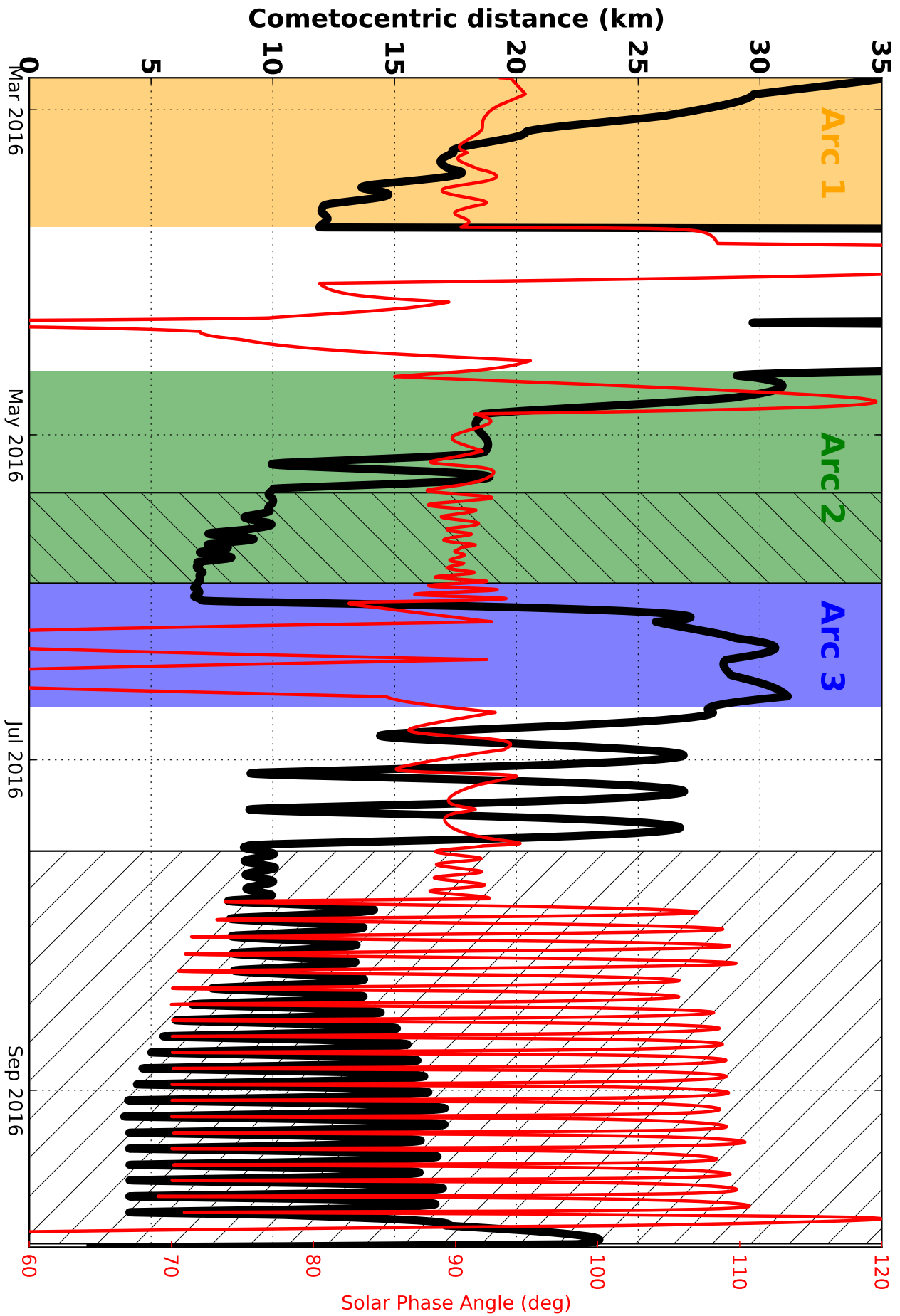


Fig. 2. Evolution of spacecraft cometocentric distance and solar phase angle in the last 7 months of Rosetta mission. The surface is at most 2.6 kilometres from the centre of mass.

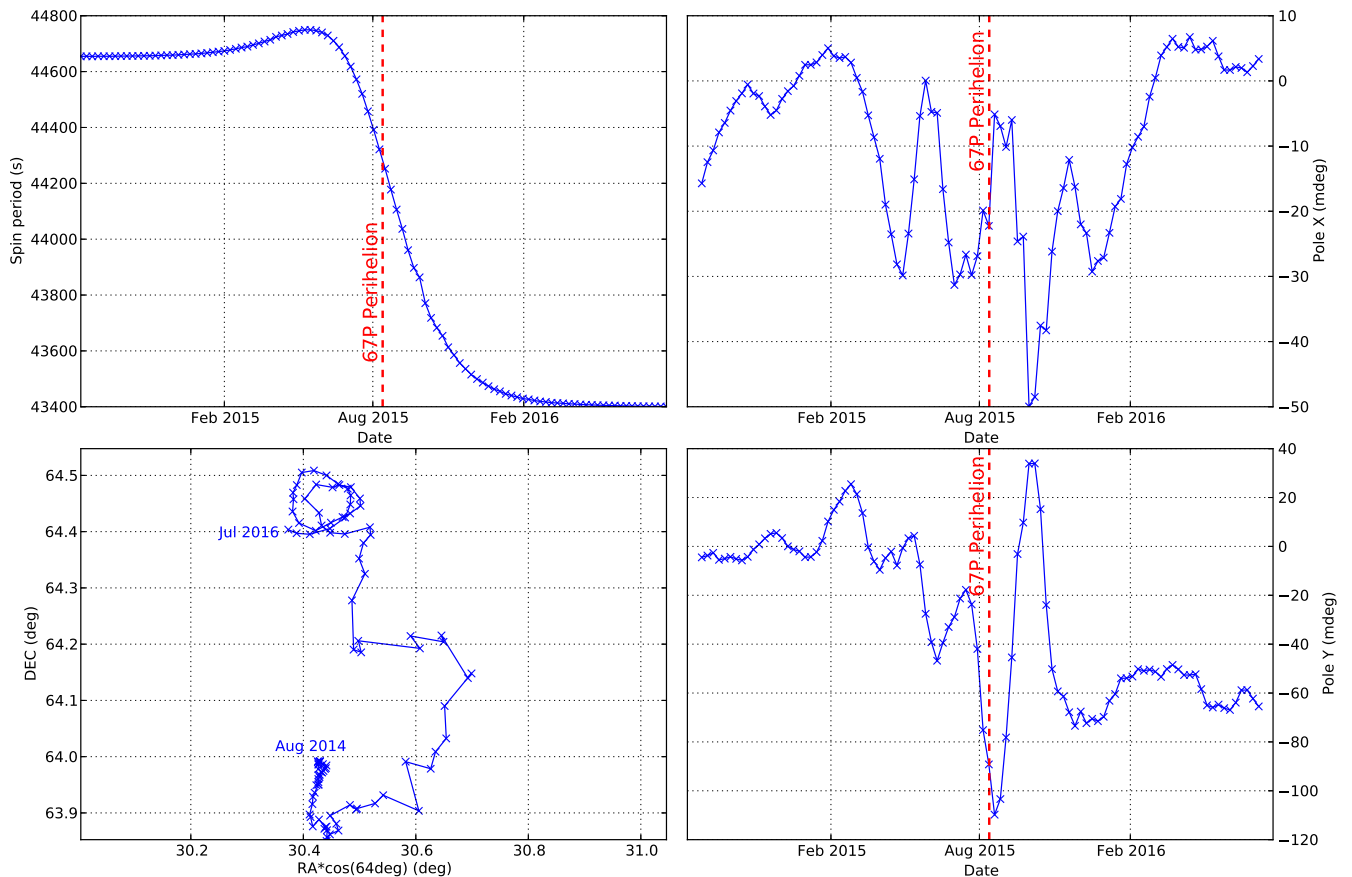


Fig. 3. Evolution of comet rotational parameters estimates from August 2014 to July 2016: Top left: spin period; Bottom left: spin direction Right Ascension (RA) and Declination (DEC) in inertial frame; Top right: spin direction offset with respect to Z along X coordinate in body frame; Bottom right: spin direction offset with respect to Z along Y coordinate in body frame. Crosses are one week apart.

The multi-arc coverage was expanded every three days. At the end of the mission, it was covering the hatched region of Fig. 2 with a total of 28 arcs. Except for the long gap between the two distinct regions, matching constraints were used between contiguous arcs.

The comet heliocentric orbit matching constraint was such that a position difference of about one meter or a velocity difference of about 0.1 millimetre per second, per axis, would lead to a normalised residual of one. Typical matching constraints post-fit residuals were of the order of a meter and 0.01 millimetre per second. It was tested that, at least for position, this could have been easily reduced to about 0.1 meter by multiplying the weight by ten without any significant impact on other residuals.

The comet attitude quaternion was constrained at the matching point so that a difference of one millidegree would produce a normalised residual of about one for each axis. The angular velocity vector was constrained such that a difference of 3×10^{-10} radians per second would lead to a normalised residual of about one per axis. The first matching constraint was such that, in practice, the difference in the comet orientation between arc was about one millidegree while the second was such that there was no significant difference in spin axis in body frame between consecutive arcs, but the spin period was decreasing slightly (0.05 to 0.2 seconds decrease every three days). Since the arcs were short enough, a uniform rotation model was used in each arc.

The spacecraft relative orbit matching constraint was such

that a difference of about one millimetre in position and 0.1 millimetre per second in velocity would produce a residual of about one per axis. Typically the observed difference between arcs was one millimetres and 0.1-0.2 millimetre per second. The matching points were chosen to coincide with momentum desaturation manoeuvres. These manoeuvres have an expected delta velocity of zero since Rosetta reaction control system is balanced and the weight of the relative velocity matching constraint was chosen according to our knowledge about the typical residual ΔV of those desaturation manoeuvres. During the fly-over phase, Rosetta was performing three desaturation manoeuvres per orbit, including one close to the apocentre which was chosen as the arc separator or matching point. The other two desaturation manoeuvres misperformance together with the pre- and post-pericentre trajectory control manoeuvres were modelled in the dynamics.

Additional constraints were added to limit the change of the coma drag acceleration scale factor between consecutive arcs. A single SRP scale factor was used for all arcs.

4.3. Results

4.3.1. Comet orbital motion

The navigation team was mainly concerned with the relative state of the spacecraft with respect to the comet, but the comet orbit was an auxiliary product of orbit determination. The determination of the orbit of 67P was complicated by the lack of knowledge of the non-gravitational forces acting on it, especially in the months around perihelion. Also in early 2015,

because the comet was in superior solar conjunction, no ground based optical measurements could be taken and the 2-way range measurements were heavily biased by the solar plasma and were not used for orbit determination.

It was observed that for Rosetta relative orbit prediction, it was better to leave the comet state free in short (about a week) orbit determination arcs than to fix it to the solution of a long arc obtained two weeks before. The resulting comet orbit was not accurate: jumps of tens of kilometres were observed between consecutive short arcs solutions. However this was sufficient for Rosetta relative navigation.

During the last month of the mission the comet was at near zero declination. In the vicinity of the Earth equatorial plane, range and Doppler observations give very little information about the comet's declination. Thus the accuracy in the comet orbit was worsened and the jumps between consecutive solutions were larger than usual.

The final comet orbit that was published for Rosetta navigation purpose is based on a propagation of the comet state obtained in the last arc of the multi-arc run described in section 4.2.. Table 1 lists the corresponding orbital parameters. The sigma values shown are from the formal consider covariance of the multi-arc solution and should not be understood as a true measure of the solution accuracy. In particular, it is to be noted that this solution was obtained using the DE405 ephemeris for the Earth and no uncertainty in Earth position was considered. Since DE405 Earth position error is probably in the order of several hundreds of meters (from a comparison with the much more recent DE432 ephemeris), the solution is likely to be biased.

4.3.2. Comet attitude motion

To monitor the evolution of the rotational state of the comet, a special orbit determination run was performed every week using a two-week long arc. This run was using fixed landmarks positions and solving for the comet rotational state assuming uniform rotational motion with no constraints on spin period

Table 1. Comet heliocentric osculating orbital elements for epoch 2016/09/25 08:51:52.3 TDB in ICRF.

Parameter	Value	Sigma
Semi-major axis (km)	518284800	78
Eccentricity	0.641717363	7×10^{-9}
Inclination (deg)	28.453633	3×10^{-5}
RA of ascending node (deg)	11.391261	4×10^{-6}
Argument of pericentre (deg)	52.643090	7×10^{-6}
True Anomaly (deg)	136.390830	1×10^{-5}

Table 2. Comet osculating rotational parameters for epoch 2016/09/25 08:51:52.3 TDB and derived quantities.

Parameter	Value	Sigma
α (deg)	69.299	0.035
δ (deg)	64.384	0.019
ω (deg)	134.767	0.036
Ω_x (rad/s)	-0.118×10^{-7}	4×10^{-9}
Ω_y (rad/s)	-0.145×10^{-6}	5×10^{-9}
Ω_z (rad/s)	$0.14477972 \times 10^{-3}$	2.5×10^{-10}
spin vector RA (ICRF)	69.401	0.031
spin vector DEC (ICRF)	64.421	0.019
spin period (s)	43398.2196	0.077

and spin vector inertial and body-fixed directions. The results of those runs are summarised in Fig. 3. Except for the spin period plot, the data was smoothed with a running average filter using 6 consecutive points. The evolution of the spin period is well observed. For the other parameters the results are very noisy. This is especially the case in 2015 when the spacecraft was flying far from the comet making it difficult to resolve the rotational motion accurately. Nevertheless, it is clear from this and from other analyses using long arc and multi-arc orbit determinations, that the spin vector direction has moved both in inertial and body-fixed frame between 2014 and 2016.

Dedicated long- and multi-arc runs were performed to assess the magnitude and frequency of the free nutation of the spin axis. For this purpose, the spherical harmonics gravitational coefficients of degree 2 were parametrized in term of the inertia tensor coefficients.²⁾ However short-term periodic motion of the spin vector due to free nutation motion could not be observed in those analyses with a resolution of a few tens of millidegrees in close orbits.

The final comet rotational state that was published for Rosetta navigation purpose is from the solution of the last arc of the multi-arc run described in section 4.2.. Table 2 lists the corresponding parameters. α , δ and ω are IAU-style rotational parameters.¹⁰⁾ However, they are not based on the true spin axis, but on the body frame Z direction with the body frame X direction for the prime meridian and thus α and δ are periodic at the comet rotation frequency. These three parameters define the body frame at epoch with respect to the International Celestial Reference Frame (ICRF), while Ω_x , Ω_y and Ω_z are the components of the angular velocity vector in body frame.

4.3.3. Comet gravity

Due to the comet shape, or rather its mass distribution, an accurate modelling of the gravitational acceleration at the altitudes flown by Rosetta in September 2016 would require a high degree and order spherical harmonics gravitational field expansion. However estimating many gravitational field coefficients results in nonsensical solutions with high variability between different observations arcs and large filter sigma for the high degree coefficients. The filter uses the freedom given by the additional coefficients to absorb other sources of mismodelling such as drag acceleration.

Figure 4 shows the evolution of the estimates for the zonal coefficients of a degree 5 order 5 gravitational field expansion for the multi-arc solution during August and September 2016. It can be seen that the J5 term changes significantly, but it also has a rather large consider sigma. The final gravitational field update is the result of that multi-arc solution. Table 3 lists the corresponding gravitational field parameters. The listed sigma values are from the formal consider covariance. Note that the effects of the uncertainty on higher degree coefficients were not considered since we do not have a measure for those uncertainties. Using the values computed from the shape model under assumption of uniform mass distribution to input rather conservative uncertainties on higher degree terms leads to much larger consider sigma. The published solution used a truncated gravitational field of degree 5 and order 5 and no a priori information for the coefficients was used. Since Rosetta flew as low as two kilometres altitude above only a few select regions of the comet

Table 3. Comet gravitational coefficients for reference radius 1 km. The coefficients are not normalised.

Parameter	Value	Sigma
GM ($km^3 s^{-2}$)	6.6592×10^{-7}	3×10^{-10}
C_{10}	+0.0060	0.0007
C_{11}	+0.0000	fixed
S_{11}	+0.0000	fixed
C_{20}	-0.5380	0.0049
C_{21}	+0.0000	fixed
S_{21}	+0.0000	fixed
C_{22}	+0.2019	0.0006
S_{22}	-0.0094	0.0006
C_{30}	-0.3735	0.0180
C_{31}	-0.1608	0.0075
S_{31}	+0.1102	0.0069
C_{32}	+0.0610	0.0014
S_{32}	-0.0328	0.0015
C_{33}	+0.0052	0.0007
S_{33}	-0.0531	0.0008
C_{40}	+0.6620	0.0938
C_{41}	-0.0555	0.0335
S_{41}	+0.0562	0.0167
C_{42}	-0.0736	0.0064
S_{42}	-0.0101	0.0032
C_{43}	+0.0012	0.0013
S_{43}	-0.0007	0.0014
C_{44}	+0.0071	0.0006
S_{44}	+0.0016	0.0006
C_{50}	+0.8252	0.3846
C_{51}	+0.1771	0.0717
S_{51}	-0.1981	0.0709
C_{52}	-0.0261	0.0130
S_{52}	-0.0226	0.0228
C_{53}	-0.0056	0.0020
S_{53}	+0.0093	0.0018
C_{54}	+0.0027	0.0005
S_{54}	-0.0007	0.0005
C_{55}	+0.0002	0.0002
S_{55}	-0.0003	0.0002

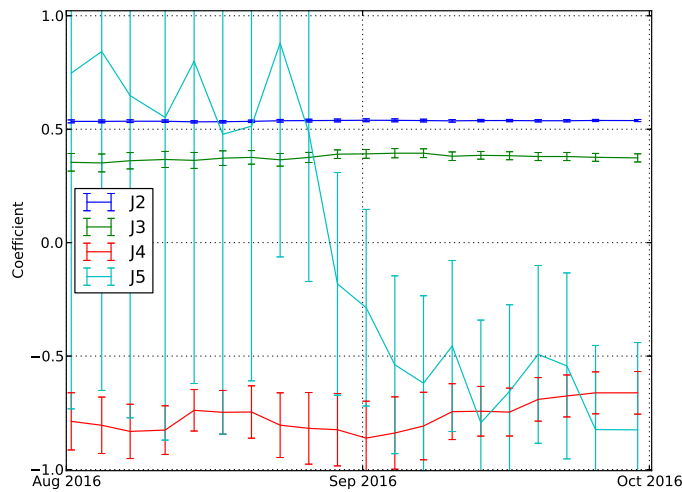


Fig. 4. Evolution of zonal coefficient estimates. Error bars correspond to one sigma formal consider covariance.

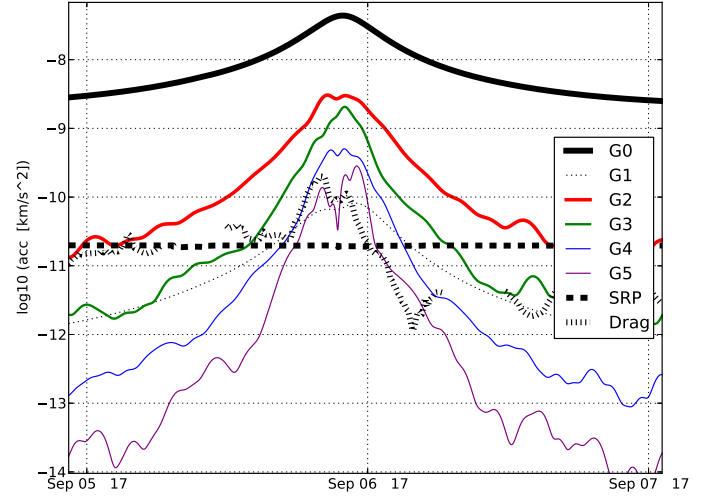


Fig. 5. Acceleration contributions for different degrees of the the gravitational field expansion, for SRP and for coma drag during a close pericentre. The plotted drag acceleration is computed from in situ static pressure measurement and thus is not covering measurement gaps.

surface, the result is likely to be biased for those regions and a different trajectory would probably have led to a different set of coefficients with a possibly large difference in the degree 5 coefficients. Figure 5 shows accelerations contribution from the different degrees of the published gravitational field around a close pericentre.

The comet GM value estimate has decreased by about 0.09% compared to 2014. While a decrease is expected due to the mass loss around perihelion, the actual amount of lost mass is difficult to assess from our solution, since the result is only about three times the formal consider sigma. The GM estimate was highly correlated to the drag scale factor estimate.²⁾

From the rotational motion, we know that the principal axis of highest inertia has rotated by about 60 millidegrees. However we did not expect to be able to observe this tiny change in the gravitational field coefficients and thus coefficients C_{21} and S_{21} were kept fixed to zero.

The centre of Mass (CoM) position is well determined in the directions orthogonal to the spin axis thanks to the rotational motion. Between 2014 and 2016 the estimate for CoM position in the XY plane changed only about 30-40 centimetres. The position of the CoM along the spin axis is however more difficult to resolve. A stronger outgassing in the southern comet regions which were lit by the Sun around perihelion should result in a “motion” of the CoM towards the North. However the change in the estimate of about 6 meters (modelled via C_{10}) towards the North is too large to be explained from the estimated comet outgassing. In any case, the change in the estimates both along the pole direction and in the equatorial plane are not significantly larger than the expected accuracy to which the CoM position can be resolved.

4.4. Modelling limitations

The limitation in the modelling of the comet orbital and rotational motions and its gravitational field were discussed in the previous section. In this section, we discuss the other main modelling limitations.

4.4.1. Coma drag

The orbit determination process estimates scale factors to the drag acceleration,²⁾ computed from the coma engineering model or in situ pressure measurements.¹¹⁾ While the engineering model software can support many different sources of gas on the comet surface, we did not have enough experimental data to configure those complex scenarios and we were always assuming the gas velocity to be directly pointing away from the comet centre. This assumption was certainly wrong during the low altitude pericentres. Fortunately, the drag acceleration was quite small in the last phase of the mission one year after perihelion, except for a few outbursts, and thus did not impact significantly the navigation accuracy.

4.4.2. Camera alignment

The landmark observations processing requires the knowledge of the spacecraft attitude as well as the alignment matrix of the current navigation camera with respect to the star tracker currently in the attitude control loop. When the star tracker is functioning nominally, the attitude follows the commanded profile within a few millidegrees and no attitude reconstruction is required. However the camera and star tracker relative alignment changes with time. This can be observed by comparing the evolution of the relative alignment between the different navigation cameras which can easily be estimated in the orbit determination process around the camera image plane axes (and with less accuracy around the boresight direction). On the other hand, the absolute alignment of a camera could only be resolved in the orbit determination to an accuracy of about 10 millidegrees around the camera image plane axes.

Because of the evolution of the camera alignment, as well as the comet environment perturbing the star tracker attitude determination, solving in the orbit determination process for the image biases per image gives obviously much better residuals. However, if too much freedom is given to those biases, most of the landmark observation information is lost and the biases are used to absorb dynamic mismodelling. Moreover in this case, the number of estimated parameters is very large and significantly slowing down the orbit determination filter. Our usual procedure was to estimate the global relative alignment between cameras over a long time interval and then use this fixed value in the orbit determination modelling the alignment biases as consider parameters with a one sigma uncertainty of 10 millidegrees.

During the orbit determination of Arc 2 of Fig. 2 a strong signature was originally observed in the landmark residuals towards the end of the arc when Rosetta was 7 kilometres from the centre of the comet. This signature could be removed by estimating a global bias of about 20 millidegrees in the cameras alignment. But an analysis of starfield images, taken in that period by the optical navigation group, showed that a global alignment bias of this magnitude was not possible. It was later understood that this signature was due to the simplifying assumption that the camera was located at the spacecraft centre of mass. This assumption had, until then, been satisfactory, but at the closer distances Rosetta was now flying this parallax effect was important. The correction was implemented in the landmark model. However, during the last two months of the mission with Rosetta flying even lower, the “improved” model

was surprisingly worsening the residuals (which were already of poor quality due to the large dynamic mismodelling at close distances). The reason could not be understood and therefore the parallax correction was not used in operations.

The uncertainty in the camera orientation is the main contributor to the comet spin direction uncertainty. It is also an important limiting factor in navigation accuracy. During the flyover phase, short term planning was based on predicted trajectories using the reconstructed state close to apocentre. The reconstructed state position is sensitive to camera orientation biases. The reconstruction accuracy (about 10 meters in the radial direction and 5 meters in the other directions) when propagated through the estimated gravitational field were leading to large post-pericentre propagation errors of the order of the observed prediction errors, not taking into account the uncertainty in the gravitational field. Hence further improvements of the gravitational field determination would likely not have improved significantly the navigation accuracy.

5. Conclusion

The decomposition of the Rosetta orbit determination problem in different arcs and different sets led to a more efficient and robust process. Taking advantage of problem sparsity and running several observation modelling programs in parallel resulted in a significant improvement in CPU time per iteration. The multiple shooting technique improved significantly the filter convergence reducing the number of required iterations.

Those techniques have been successfully applied to determine the physical parameters of comet 67P to an accuracy that met the most demanding requirements of Rosetta navigation close to the comet in the last months of the mission.

References

- 1) Accomazo, A., Ferri, P., Lodi, S., Pellon-Bailon, J-L., Hubault, A., Urbanek, J., Kay, R., Eiblmaier, M. and Francisco, T.: The Final Year of the Rosetta Mission, *Acta Astronautica*, **136**(2017), pp. 354–359.
- 2) Godard, B., Budnik, F., Muñoz, P., Morley, T. and Janarthanan, V.: Orbit Determination of Rosetta around Comet 67P/Churyumov-Gerasimenko, 25th International Symposium on Space Flight Dynamics, Munich, 2015, http://issfd.org/2015/files/downloads/papers/124_Godard.pdf (accessed April 3, 2017).
- 3) Muñoz, P., Companys, V., Budnik F., Godard, B., Pellegrinetti, D., Bellei, G., Bauske, R. and Martens, W.: Rosetta Navigation during the End of Mission Phase, 26th International Symposium on Space Flight Dynamics, Matsuyama, 2017 (expected).
- 4) Bierman, G.J.: *Factorization Methods for Discrete Sequential Estimation*, Dover Publications, New York, 1977.
- 5) Bierman, G.J.: Householder Orthogonal Transformations, *Factorization Methods for Discrete Sequential Estimation*, Dover Publications, New York, 1977, pp. 57–67.
- 6) Scheeres, D.J.: Failure Modes of Reduced-Order Orbit Determination Filters and Their Remedies, *The Telecommunications and Data Acquisition Report*, 1993, pp. 34–42, <https://ntrs.nasa.gov/archive/nasa/casi.ntrs.nasa.gov/19940009900.pdf> (accessed April 3, 2017).
- 7) SciPy.org website, <https://www.scipy.org/> (accessed April 9, 2017).
- 8) Multiprocessing library, Python Documentation website, <https://docs.python.org/2/library/multiprocessing.html> (accessed April 9, 2017).
- 9) Pardo de Santayana, R. and Lauer, M.: Optical Measure-

ment for Rosetta Navigation near the Comet, 25th International Symposium on Space Flight Dynamics, Munich, 2015, <http://issfd.org/2015/files/downloads/papers/062.Pardo.pdf> (accessed April 16, 2017).

- 10) Archinal, B.A., A'Hearn, M.F., Bowell, E., Conrad, A., Consolmagno, G.J., Courtin, R., Fukushima, T., Hestroffer, D., Hilton, J.L., Krasinsky, G.A., Neumann, G., Oberst J., Seidelmann, P.K., Stooke, P., Tholen, D.J., Thomas, P.C. and Williams, I.P.: Report of the IAU Working Group on cartographic coordinates and rotational elements: 2009, *Celestial Mechanics and Dynamical Astronomy*, 2010, pp. 101–135, <http://aa.usno.navy.mil/publications/reports/Archinaletal2011a.pdf> (accessed April 16, 2017).
- 11) Bielsa, C., Müller, M. and Herfort, U.: Operational Approach for the Modelling of the Coma Drag Force on Rosetta, 24th International Symposium on Space Flight Dynamics, Laurel, 2014, http://www.issfd.org/ISSFD_2014/ISSFD24_Paper_S11-2_Bielsa.pdf (accessed April 16, 2017).